

Supporting Information

Biomimetic Hierarchical Assembly of Helical Supraparticles from Chiral Nanoparticles

Yunlong Zhou,^{†,‡} Ryan L. Marson,^{§,||} Greg van Anders,^{†,§} Jian Zhu,[†] Guanxiang Ma,[†] Peter Ercius,[#] Kai Sun,^{||} Bongjun Yeom,^{†,¶} Sharon C. Glotzer,^{*,†,§,||} Nicholas A. Kotov^{*,†,§,||,⊥}

[†]Department of Chemical Engineering, [§]Biointerfaces Institute, ^{||}Department of Materials Science and Engineering, [⊥]Department of Biomedical Engineering, University of Michigan, Ann Arbor, Michigan 48109, United States

[‡]Wenzhou Institute of Biomaterials and Engineering, CNITECH.CAS-Wenzhou Medical University, Wenzhou, Zhejiang 325011, People's Republic of China

[#]National Center for Electron Microscopy, the Molecular Foundry, Lawrence Berkeley National Laboratory, Berkeley, California 94720, United States

[¶]Department of Chemical Engineering, Myongji University, Yongin, Gyeonggido 17058, South Korea

*Email: sglotzer@umich.edu; kotov@umich.edu

Part I: Experimental Results

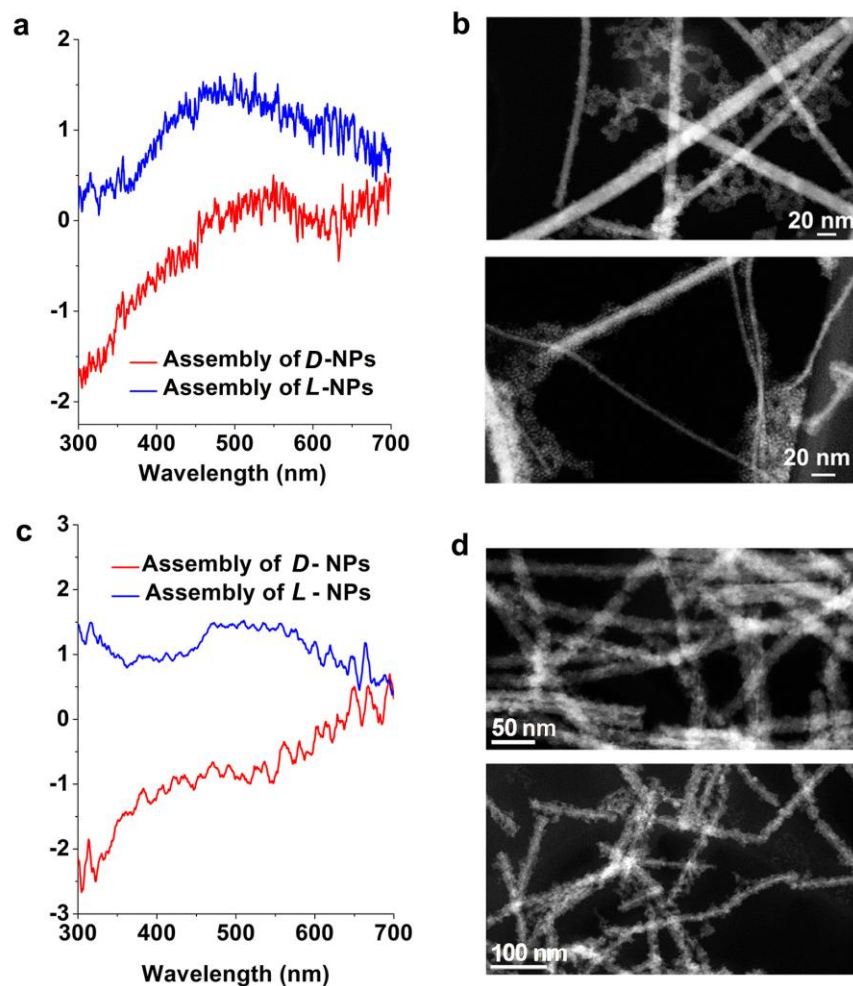


Figure S1. CD spectra and corresponding STEM HAADF images for assemblies made in sub-optimal conditions. (a, b): Insufficient attachment of NPs to the surface of core Te NRs; (c, d): Over dense NPs attached on the surface of the core Te NRs with more random arrangement due to aggregation in low pH value. (Top STEM HAADF image: assembly of *D*-NPs; Bottom STEM HAADF image: assembly of *L*-NPs)

The formation of chiral helical assemblies is critically influenced by the pH value and the efficiency of oxygen removal, which both are key factors to the assembly under the control of thermodynamics. The assembly should conduct under Te^{2-} release and the formation of Te NRs

in a very slow rate, and avoid NP decomposition due to the serious oxidation of NPs. The assembly conducting in open atmosphere formed long Te nanowires (NWs) irregularly attached NPs as well as some Te NWs with large diameter (Figure S1 a, b). It is because that the NPs decomposed quickly and too much Te NWs formation unbalanced the interaction force among of NPs. Figure (S1 c, d) however, indicated the assembly conducted in pH value at 11.0. The NPs released few of Te^{2-} and stacked NP chains attached irregularly on the surface of Te mainly driven by van der Waals forces. Therefore, the highly condensed NPs stacks on the Te wires are more like a core-shell structures. The achiral structures for the assemblies under high content of oxygen and high pH value were also indicated two broad asymmetric signals in the CD spectra.

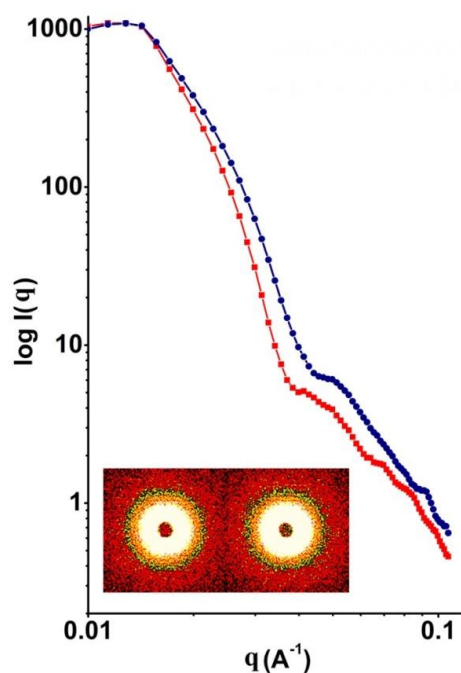


Figure S2. Small angle X-ray scattering characterization of *left*- (red) and *right*- (blue) hand helical NRs. The d spacing is calculated by $d=2 \pi/q$, which is 12.6 nm.

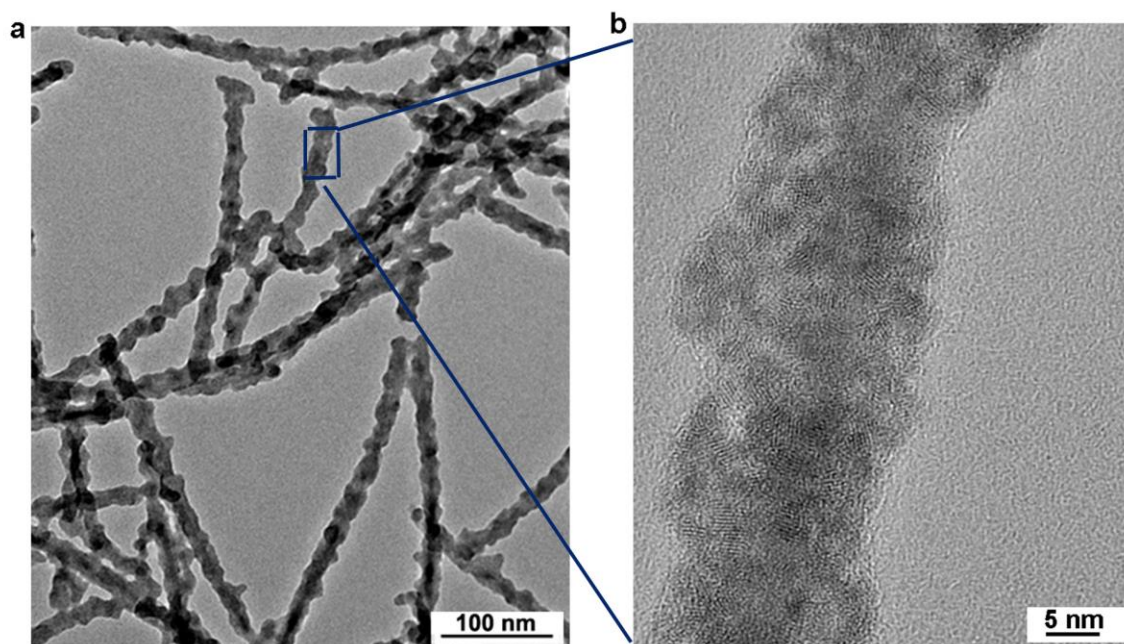


Figure S3. TEM BF (left) and HREM (right) images of right- handed helical assemblies from *L*-NPs.

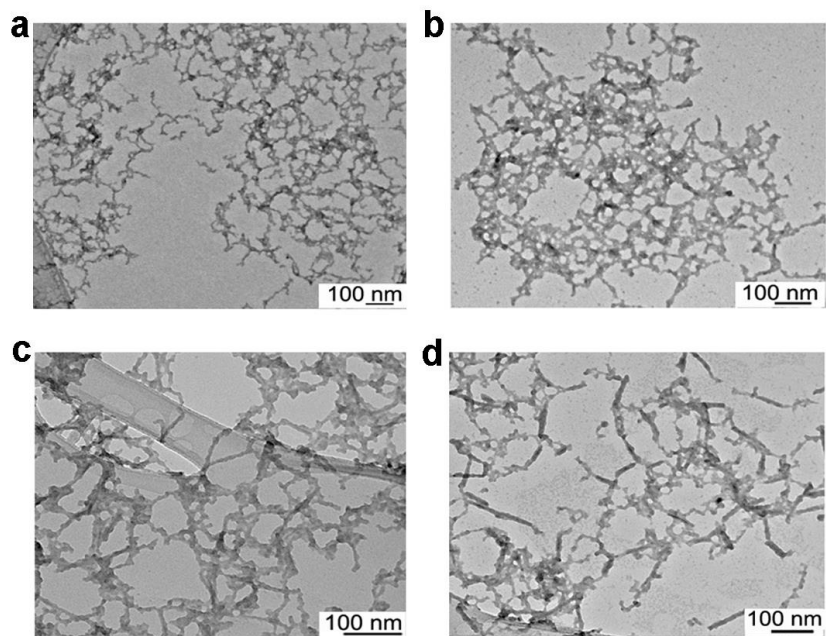


Figure S4. Intermediate states of assembly of *L*-NPs. (a-d) TEM BF images of the formation process of *right*-hand helical structures by assembly of *L*-NPs in 8 hours (a), 24 hours (b), 48 hours (c) and 72 hours (d).

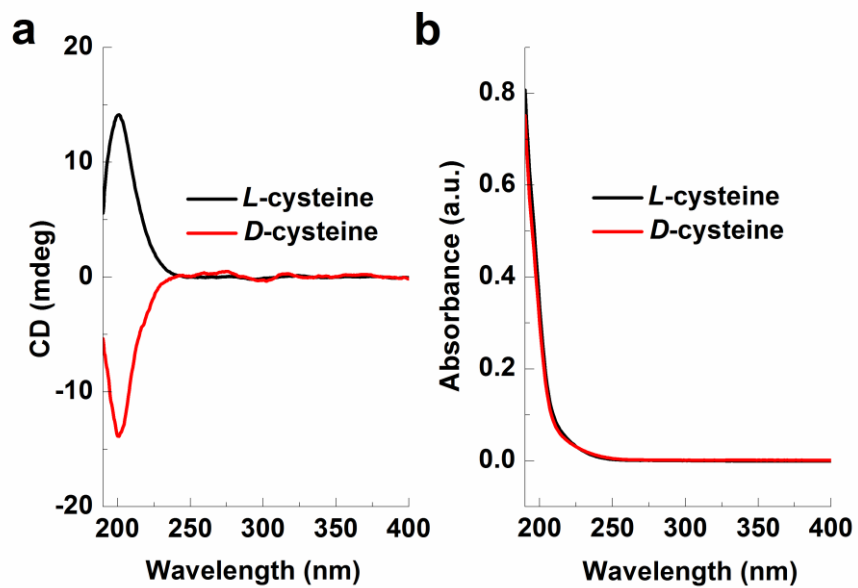


Figure S5. CD and UV-vis spectra of (*D* and *L*) cysteine.

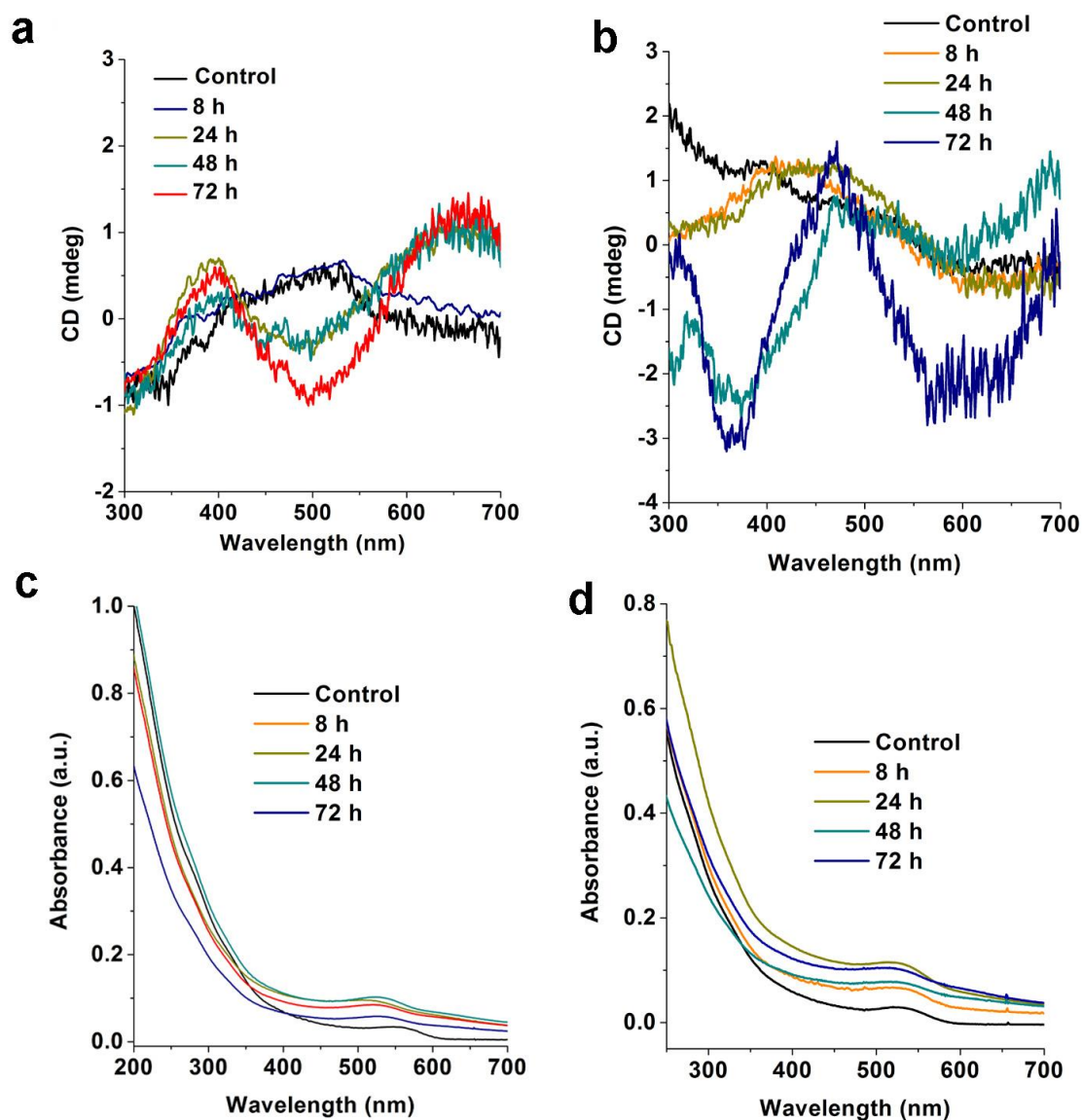


Figure S6. CD and UV-vis spectra of NP dispersions representing different intermediate stages of assembly of supraparticle helices. Control sample represents free NPs before the assembly. **(a, c)** The process of formation of *left*-handed helices assembled from *D* - NPs during 72 h. **(b, d)** The process of formation of *right*-handed helices assembled from *L* - NPs during 72 h.

As shown in Fig. S6 c,d, the UV-vis spectra show minor red-shift, which means the NP size essentially unchanged in the formation of assemblies. Therefore, we could evaluate the NP size

and dipole moment based on the first excitonic absorption peak of NPs. The calculated size of CdTe NPs is 3.2 nm based on the followed equation in reference: ¹

$$\Delta E_g = a_1 e^{-d/b_1} + a_2 e^{-d/b_2}$$

$$\Delta E_g = E_{gQD} - E_{g0}$$

For CdTe NPs, where $E_{g0} = 1.61 \text{ eV}$, d is the diameter of the CdTe NPs, $a_1 = 5.77$, $b_1 = 8.45$, $a_2 = 1.33$, $b_2 = 43.73$. Where E_{gQD} is band gap of NPs obtained from the wavelength of the first excitonic absorption peak, and E_{g0} is bulk band gap. The first excitonic absorption peaks for NP used is $\sim 525 \text{ nm}$.

The energy of dipole attraction between CdTe nanoparticles can be calculated with followed equation:

$$E = -\mu^2 / 2\pi\epsilon_0 r (r^2 - d_{np}^2), \epsilon_0 = 8.85 * 10^{-12} \text{ C}^2 \text{ J}^{-1} \text{ m}^{-1}.$$

The center-to-center interdipolar separation r is $\sim 4.2 \text{ nm}$ and $\mu = 50 \text{ D}$ for nanoparticle diameter $d_{NP} \sim 3.2 \text{ nm}$, the energy of nanoparticle dipole attraction is equal to 9.7 kJ/mol .

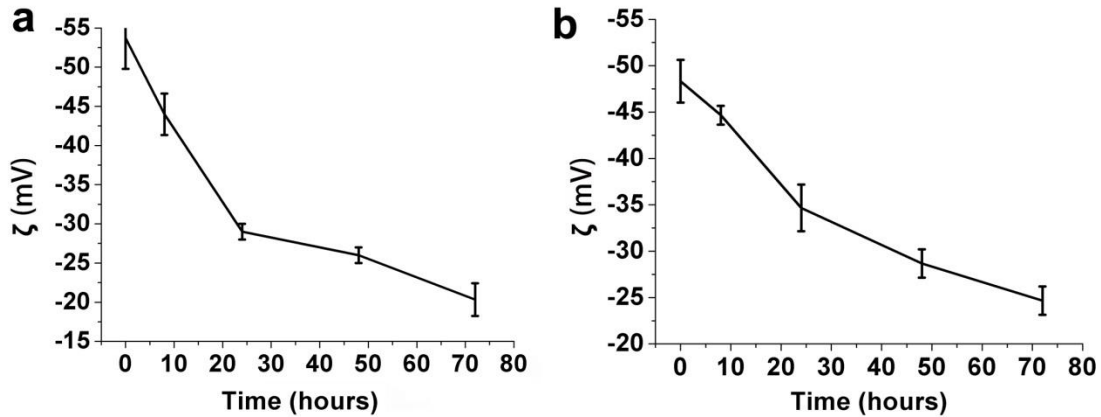


Figure S7. Zeta potential, ζ , of (a) *D*-NPs and (b) *L*-NPs assemblies.

The zeta potential of NPs assemblies dramatically decreased in the intermediate state of the formation of helices. It is attributed to the gradually formation of chiral CdTe aggregation on the surface of Te NRs. As we can see from the TEM images in Fig. 4 in the main manuscript, the formation of NP chains and helical NRs are the results of chiral arrangement of NPs.

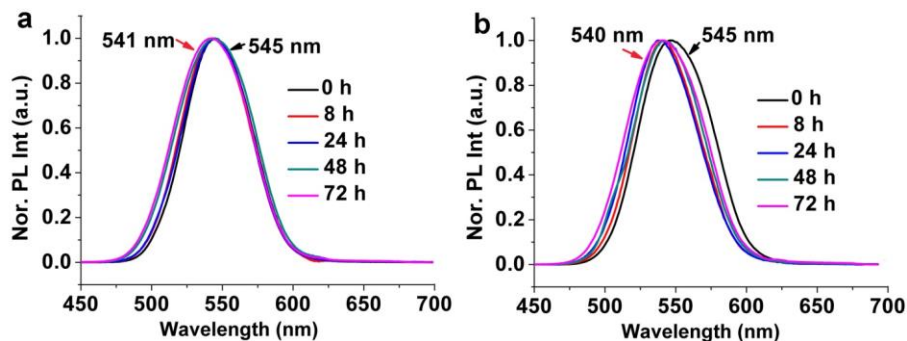


Figure S8. PL spectra for the assemblies of (a) *D*-NPs and (b) *L*-NPs.

The formation of NP chains and helical assemblies result in red-shift of the PL peaks. In contrast, the oxidation of NPs contributes blue-shifted PL peaks. In the formation of the NP helical superstructures, the chiral arrangement of NPs and oxidation of NPs occurred under synchronous, which is the counteraction effect of blue-shifted and red-shifted PL peaks. Therefore, we did not observe either strong blue-shifted or red-shifted effect in the intermediate states.

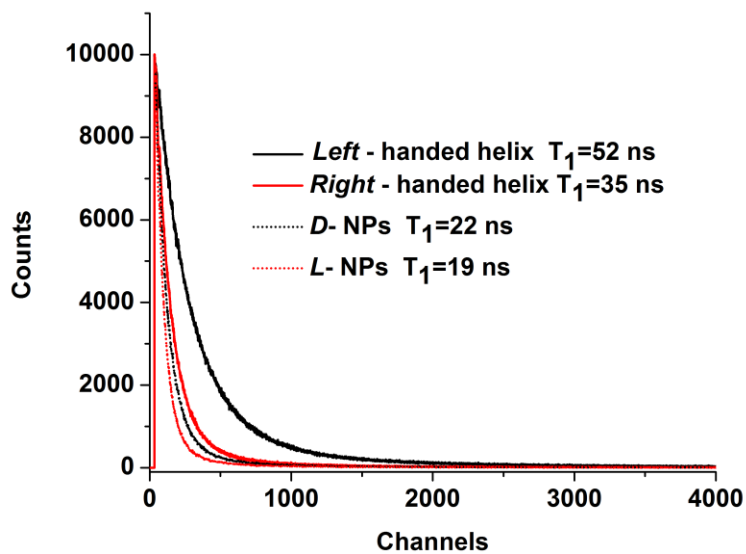


Figure S9. PL lifetime characterization of (*D*-, *L*-) NPs and corresponding *left*- and *right*- hand helix.

PL lifetimes were studied using a JY-Horiba FluoroLog-3 time resolved fluorimeter. The PL decay was adopting three exponential functions by DAS6 Fluorescence Decay Analysis Software. The radiative lifetime of (*D*-, *L*-) NPs and corresponding *left*- and *right*- handed helix showed some characteristic room temperature fluorescence decay curves.

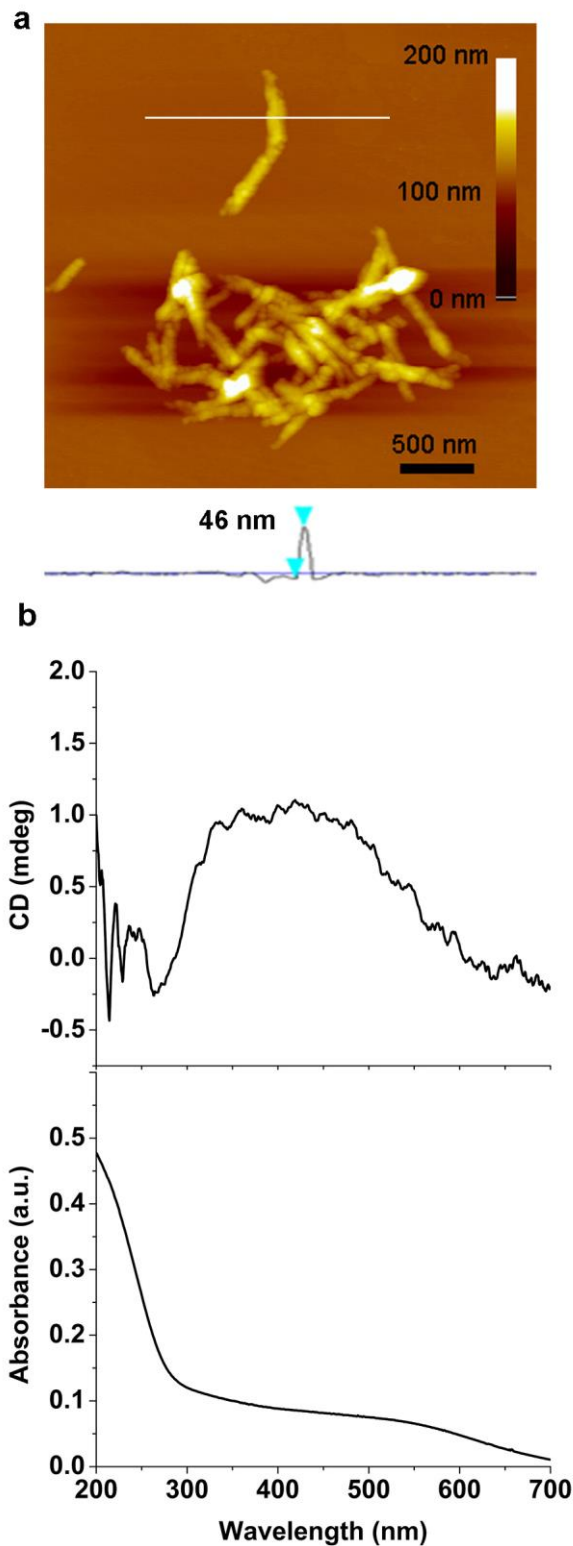


Figure S10. CD/ UV-vis spectra and AFM height image of fibers obtained from self-assembly of *rac* – NPs.

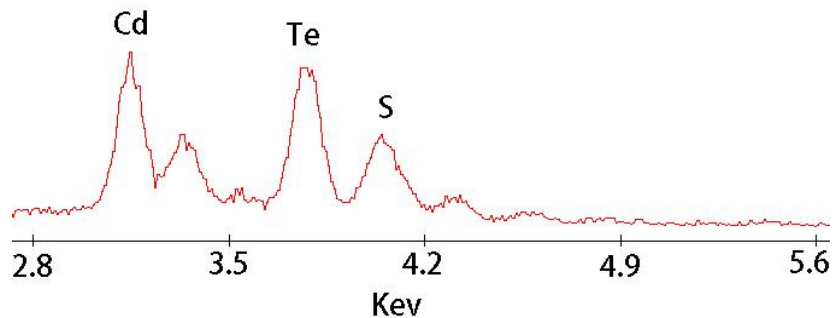


Figure S11. XEDS analysis of fibers obtained from self-assembly of *rac* – NPs.

Part II Simulation Model and Methods

Brownian Dynamics

Systems are simulated in an implicit solvent within the NVT ensemble, using Brownian Dynamics (BD).²

To mimic the assembly forces present in the system, we use a cylindrical harmonic well of the form $U = \frac{1}{2}kx^2$ (where x denotes the radial distance from the center of the box). This provides a linear driving force toward the z -axis of the box. The strength of attraction to the z -axis can be tuned *via* the spring constant, k . At $k = 0$, the field has no effect, allowing the particles to diffuse freely throughout the box. As the strength of k is increased, the particles begin to aggregate; at values of $k = 10$ and above particles are confined to the surface of the rod. The width of this aggregation region can be made arbitrarily wide by scaling the distance by a preferred value (x/x_0), or be made flat by generalizing the exponent to $2N$. Rods are placed along the z -axis of the box to provide a steric hindrance, mimicking the effect of the rigid Te core around which

nanoparticle assembly occurs. The diameter of the inner Te core was chosen to match experiment, 1 and 2 NP widths.

Simulations are initialized with particles placed on a simple cubic grid in a periodic, cubic box. The system is randomized by raising the temperature well above the order-disorder transition temperature, $T^* \gg T^{\text{ODT}}$ for 1 million time steps. All simulations use a $\Delta t = 0.005\sqrt{m\sigma^2/\varepsilon}$ time step. Simulations were performed at a variety of conditions – varying particle number ($N = 100 - 300$), spring constant ($k = .001$ to 10), and twist strength ($\varepsilon = 0 - 100$).

Each state point was run in 5 independent simulations, equally spaced between $N = 100$ and 300 nanoparticle. Simulations begin at $k = 0.001$, and are ramped up to $k = 10.0$ over 10^6 time steps. The twist parameter begins at a finite, non-zero value ($\varepsilon = 1.0, 10.0, \text{ or } 100.0$) in simulations with the chiral pair force, and is increased by two orders of magnitude over an additional 10^6 time steps. Finally, systems are equilibrated for an additional 100^6 time steps and the resulting configurations are averaged over the run before analyzing.

Discrete Element Method

Previous computational investigations of truncated tetrahedra have been carried out by modeling particles with stacked spheres.³⁻⁵ Because our investigation is focused on determining whether nanowire chirality is sensitive to cysteine chirality, we wanted to eliminate any effects that could arise from the interdigitation that can occur in stacked sphere models. To eliminate these effects, a modified version of the Discrete Element Method (DEM), adopted from the granular community, is used to simulate the truncated tetrahedron shape of the nanoparticle.⁶ This avoids the need to stack Weeks-Chandler-Andersen (WCA) spheres to create the

nanoparticle shape, thus creating a smoother surface that avoids artifacts due to interdigitation or compounding energy effects.⁷

In DEM, contact forces are determined by summing over the geometric features of the shape - vertices, edges, and faces. Between a pair of particles, all pairs of features are checked against each other. From these distance checks, a force is calculated if features are close enough to interact based upon the chosen pair potential. Forces and torques are calculated between all pairs of geometric features -

$$\vec{F}_{ij} = \sum_{E_i, E_j} \vec{F}(E_i, E_j) + \sum_{V_i, F_j} \vec{F}(V_i, F_j) + \sum_{V_j, F_i} \vec{F}(V_j, F_i)$$

To evaluate energies, forces, and torques between particles we must first find distances between pairs of geometric features (G) -

$$d(G_1, G_2) = \|\vec{Y} - \vec{X}\|$$

where \vec{X} and \vec{Y} represent the closest points between two features, which are chosen using standard point-point, point-line, and point-plane formulae such as those available at <http://www.geometrictools.com>.

We model excluded volume (steric) forces between particle features using a Weeks-Chandler-Anderson (WCA) potential⁸:

$$V_{ij}^{SLJ}(r) = 4\epsilon_{ij} \left[\left(\frac{\sigma_{ij}}{r-\delta} \right)^{12} - \left(\frac{\sigma_{ij}}{r-\delta} \right)^6 \right]$$

$$U_{ij}^{WCA}(r) = \begin{cases} V_{ij}^{SLJ}(r) - V_{ij}^{SLJ}(r_{cut}^{WCA}) & r < r_{cut}^{WCA} + \delta \\ 0 & r \geq r_{cut}^{WCA} + \delta \end{cases}$$

where $r_{cut}^{WCA} = 2^{\frac{1}{6}}$ is the cut off.

Dipoles

We studied model systems of particles both with and without screened electric dipoles, which we modeled as has been reported in prior work.^{5, 9} Some modifications to the original parameters were made to account for the different dimensionless scale of the DEM model to stacked spheres. The charge and dipole moment is specified in reduced units as $q^* = q/(4\pi\epsilon_0\sigma\epsilon)^{1/2} = +1.0$ and $m^* = m/(4\pi\epsilon_0\sigma^3\epsilon)^{1/2} = 20.0$.

Chiral Pair Potential/Force

To include the “twisting” effect induced by the amino acid stabilizer, we include a pair potential that acts between faces of the truncated tetrahedra. We calculate and apply a chiral potential between the faces of a pair of tetrahedra, i and j as follows: We take our particles to

have hexagonal face normals \hat{z}_a and face orientations \hat{w}_a given by

$$\begin{aligned} \hat{w}_1^i &= \frac{1}{\sqrt{6}}(1, -2, 1) & \hat{w}_2^i &= \frac{1}{\sqrt{6}}(-1, 2, 1) & \hat{w}_3^i &= \frac{1}{\sqrt{6}}(-1, -2, -1) & \hat{w}_4^i &= \frac{1}{\sqrt{6}}(1, 2, -1) \\ \hat{z}_1^i &= \frac{1}{\sqrt{3}}(1, 1, 1) & \hat{z}_2^i &= \frac{1}{\sqrt{3}}(-1, -1, 1) & \hat{z}_3^i &= \frac{1}{\sqrt{3}}(-1, 1, -1) & \hat{z}_4^i &= \frac{1}{\sqrt{3}}(1, -1, -1) \end{aligned}$$

Given two particles i and j that are within range to interact (their centers of mass are within some cut-off distance) we iterate through their hexagonal faces (a,b), and impose a "twist" to pairs of interacting faces that we encode through the quantity $\xi_{ab}^{ij} = \frac{1}{2}(\hat{w}_a^{i'} \times \hat{w}_b^{j'}) \cdot (\hat{z}_a^{i'} - \hat{z}_b^{j'})$, where the primes indicate the rotation of the particles from their base orientation to the lab frame. The faces interact with a potential that is a function of both the distance between face centers and the twist that is given by

$$U_\chi(r_i, r_j, q_i, q_j) = \sum_{ab} \tilde{U}_{ab}^{ij}(r_{ab})(3\xi_{ab}^{ij} - 4\xi_{ab}^{ij3})$$

where the dependence on the radial distance between faces has the Hertzian form

$$\tilde{U}_{ab}^{ij}(r_{ab}) = \begin{cases} \epsilon_\chi \left(1 - \frac{r_{ab}}{\lambda}\right)^{\frac{5}{2}} & r_{ab} < \lambda \\ 0 & r_{ab} \geq \lambda \end{cases}$$

To model the racemic stabilizer mixture we use the potential

$$U_{\bar{x}}(r_i, r_j, q_i, q_j) = \sum_{ab} \tilde{U}_{ab}^{ij}(r_{ab}) \left(4(1 - \xi_{ab}^{ij2})^{3/2} - 3(1 - \xi_{ab}^{ij2})^{1/2} \right)$$

For fixed *L*- or *D*-Cys, the twist dependent modulation of the potential is designed so that when $\hat{z}_a^{i'} = -\hat{z}_b^{j'}$ particle faces are aligned, the potential imparts a preferential angle misalignment of the hexagons of the form $\sin(3\theta)$ that is determined by the sign of ϵ_x as shown below. For the racemic mixture, the twist dependent modulation of the potential is designed so that the preferential alignment has the form $\cos(3\theta)$ when the face normals are antiparallel.

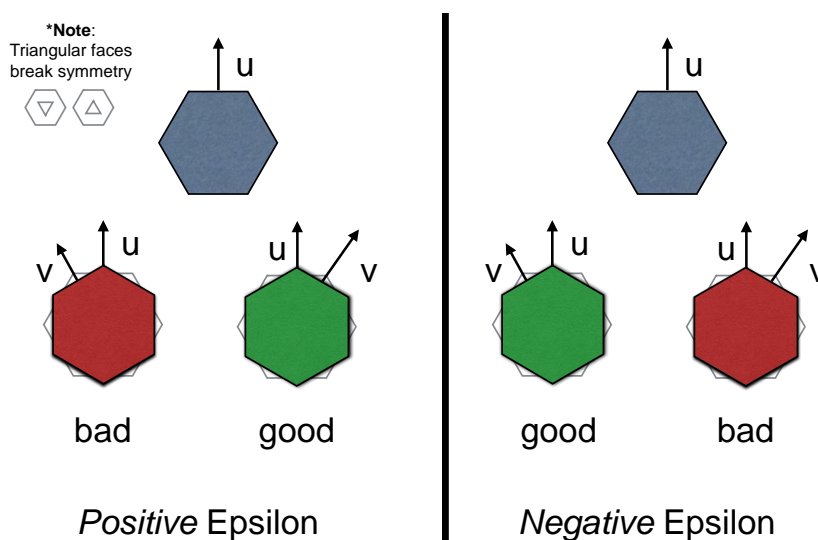


Figure S12. Modeling of chiral interaction and NP-NP interfaces. A chiral potential induces a local bias, or twist, between pairs of nanoparticles. The sign of epsilon in the potential determines the direction of the local twist. The preference is shown relative to the hexagonal faces of the truncated tetrahedra; positive epsilon results in a right twist, while negative epsilon produces a left twist. The strength of the chiral interaction 4.1 kJ/mol was calculated by

$(\epsilon)_{\text{kJ/mol}} = (\epsilon)k_B T \frac{10^3}{N_A(T_R)_K(k_B)_{\text{J/K}}}$. Here, $(T_R)_K$ is room temperature (20 °C) in units of Kelvin,

N_A is Avogadro's number, $(k_B)_{\text{J/K}}$ is Boltzmann's constant (in units of Joules per Kelvin), and 10^3 converts to kJ rather than Joules.

REFERENCES AND NOTES:

1. Sapra, S.; Sarma, D. D. Evolution of The Electronic Structure with Size in II-VI Semiconductor Nanocrystals. *Phy. Rev. B* **2004**, *69*, 125304.
2. Grest, G. S.; Kremer, K. Molecular Dynamics Simulation for Polymers in The Presence of a Heat Bath. *Phy. Rev. A* **1986**, *33*, 3628-3631.
3. Tang, Z.Y.; Wang, Y.; Sun, K.; Kotov, N. A. Spontaneous Transformation of Stabilizer-Depleted Binary Semiconductor Nanoparticles into Selenium and Tellurium Nanowires. *Adv. Mater.* **2005**, *17*, 358-363.
4. Park, J. I.; Nguyen, T. D.; de Queirós Silveira, G.; Bahng, J. H.; Srivastava, S.; Zhao, G.; Sun, K.; Zhang, P.; Glotzer, S. C.; Kotov, N. A. Terminal Supraparticle Assemblies from Similarly Charged Protein Molecules and Nanoparticles. *Nature Commun.* **2014**, *5*, 3593.
5. Zhang, Z.L.; Tang, Z.Y.; Kotov, N. A.; Glotzer, S. C. Simulations and Analysis of Self-Assembly of CdTe Nanoparticles into Wires and Sheets. *Nano Lett.* **2007**, *7*, 1670-1675.
6. Ghaboussi, J.; Barbosa, R. Three-Dimensional Discrete Element Method for Granular Materials. *Inter. J. Numer. Anal. Methods in Geomechanics* **1990**, *14*, 451-472.
7. John, B. S.; Stroock, A.; Escobedo, F. A. Cubatic Liquid-Crystalline Behavior in A System of Hard Cuboids. *J. Chem. Phys.* **2004**, *120*, 9383-9389.
8. Chandler, D.; Weeks, J. D.; Andersen, H. C. Van der Waals Picture of Liquids, Solids, and Phase Transformations. *Science* **1983**, *220*, 787-794.
9. Tang, Z.Y.; Kotov, N. A.; Giersig, M. Spontaneous Organization of Single CdTe Nanoparticles into Luminescent Nanowires. *Science* **2002**, *297*, 237-240.